show an isotropic energy gap in the ab plane.[32] Also the PES results displayed a larger gap than the predicted weak-link BCS theory, although the temperature dependence was similar. The energy gap has also been measured using tunneling and Andreev reflection methods.[24,25]

1.2.2 Superconducting $YBa_2Cu_3O_{7-\delta}$

1.2.2.1 Structure of Yttrium Barium Copper Oxide ($YBa_2Cu_3O_{7-\delta}$)

Most of the high–T_c structures are Perovskite[33] based tetragonal or nearly tetragonal, (having a small orthorhombic or other distortion), however, the $YBa_2Cu_3O_{7-\delta}$ structure with $\delta << 1$ is predominantly orthorhombic. Figure 1.2.1a shows the skeleton structure for $YBa_2Cu_3O_{7-\delta}$ (YBCO). For this material, there are two immediately adjacent Cu–O planes (≈3.2Å apart), and these two Cu–O planes (n=2) are greater than 8.2 Å from the next two Cu–O planes. The three metal–O isolation planes that separate the two immediately adjacent Cu–O planes in YBCO are also indicated.

YBCO is a complicated structure because of its variable oxygen content and two different types of four coordinated Copper atoms. Figure 1.2.1b represents the orthorhombic YBCO structure and emphasizes the labelling of the atom positions. The Cu–O planes extend indefinitely in two directions (the ab plane), while the Cu–O chains extend indefinitely in only one direction (the b direction). The atomic spacing of the tetragonal YBCO (123) system is a ≃ b ≅ 3.9 Å, c ≅ 11.8 Å. The $YBa_2Cu_3O_{7-\delta}$ structure has a T_c of 90 K. When the oxygen content is reduced in the Cu–O chains T_c decreases and superconductivity disappears for $\delta > 0.5$ where the antiferromagnetic insulator $YBa_2Cu_3O_6$ begins to form.

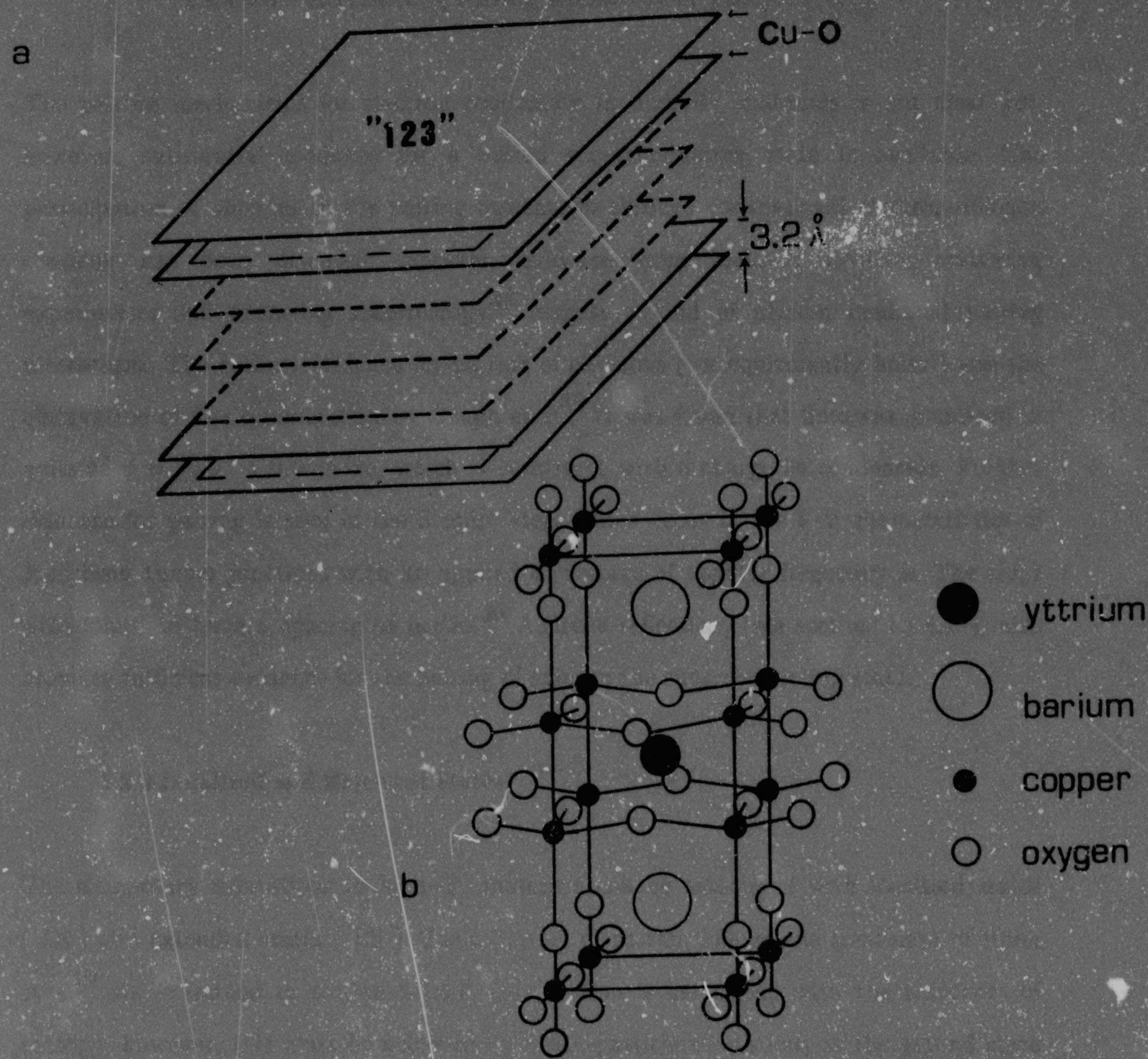

Figure 1.2.1 (a) A schematic representation of the YBCO structure emphasizing the two immediately adjacent Cu–O planes. The sparsely occupied Y–atom plane between the adjacent Cu–O planes is indicated by a light dashed line. The three other (isolation) metal–O planes are indicated by heavier dashes. (b) Orthorhombic YBCO emphasizing the atomic positions

1.2.2.2 Superconducting Pairing Mechanism of $YBa_2Cu_3O_{7-\delta}$

The pairing mechanisms for electron condensate in high–T_c materials is not clear yet, however, substantial evidence for a paired superconducting state is available. The participation of phonons in the pairing mechanism through conventional electron–phonon coupling has been disputed, however, evidence from inelastic neutron scattering experiments and tunneling spectroscopy[34] suggest a kind of phonon mediated pairing mechanism. The earliest evidence for pairing of electrons (or equivalently holes) was the observation of flux quantization by Gough et al.[35] It was found that flux was quantized in units of $\psi = (0.97 \pm 0.04)h/2e$, which is consistent with a charge 2e condensate. Further evidence for pairing is seen in the Shapiro steps which occur in the I–V characteristics of Josephson tunnel junctions with an applied ac voltage of angular frequency ω. The steps were found to have a spacing of $h\omega/2e$.[36] Andreev reflection, (see section 1.1.4.1), also provides sufficient evidence for the pairing of holes in the superconducting state.

1.2.3 Localized and Extended States

The elementary excitations in high–T_c materials can be associated with **localized states** (LS) and **extended states** (ES). The following discussion follows the treatment of Hohn et al.[37] As examined in section 1.1.4.3, flux motion is associated with the transport of entropy, however, this must be achieved by quasi–particle excitations as the ground state superfluid does not carry any entropy. Figure 1.2.2 shows the spatial variation of the order parameter from the centre of a flux–line. The order parameter and energy gap have a finite value Δ_∞ in the bulk superconductor, dependent on the temperature and magnetic field. There exist in the mixed state two types of quasi–particle excitations:

i) **Localized states** or bound excitations with energy, $\epsilon < \Delta_\infty$ that are situated inside the vortex core at regular energy spacings of $\hbar^2/2m\xi^2$.

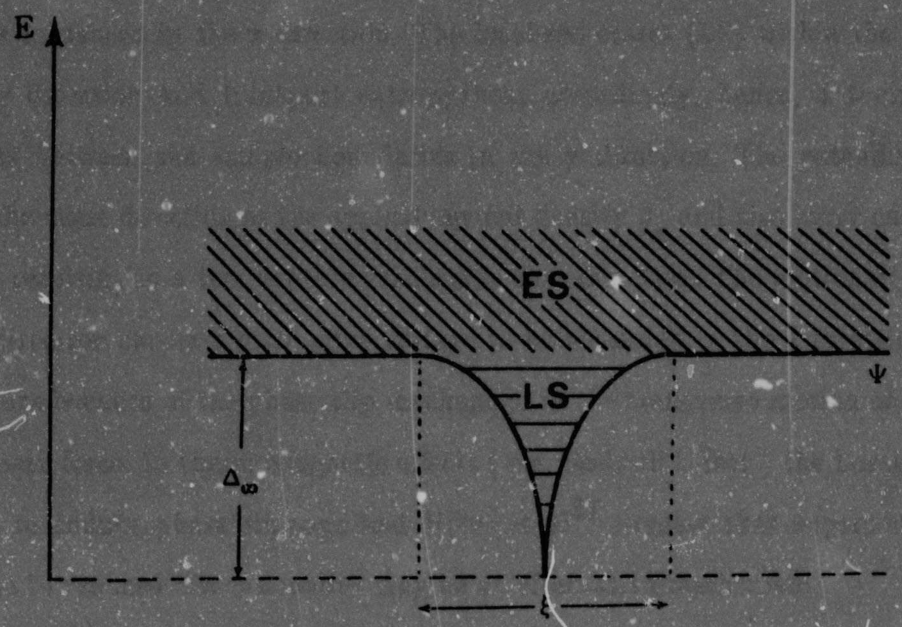

Figure 1.2.2 Variation of the superconducting order parameter Ψ, it is zero in the centre of a vortex and rises to its maximum value within a distance of the coherence length, ξ. In the core there are bound quasi–particle excitations (Localised States) and Excited states outside the core that are not bound.

ii) **Extended states** or unbound excitations with energy $\epsilon > \Delta_\infty$ that spread throughout the superconducting sample in an analogy to the 'normal' density in the Two Fluid model.

Consider the superconducting circuit in figure 1.2.3. Applying a transport current in the x direction and an applied magnetic field in the z direction causes a vortex motion in the y direction, due to the Lorentz force. Neglecting the Hall voltage contribution, the resulting voltage drop is measured in the x direction. The localized states (LS) within the vortices move in the y direction and transport entropy/heat accordingly, hence, a temperature gradient results between the sample boundaries in the y direction. The extended states (ES) move in the same direction as the applied current density J_x and also carry entropy in the x direction resulting in a temperature gradient in that direction. The motion of vortices (LS) in the y direction causes a dissipative voltage to be measured in the x direction. This dissipation occurs because of the phase slip mechanism in the transverse motion of vortices due to the Lorentz force. In thermomagnetic effects (e.g. Seebeck Effect) the Lorentz force is not present to induce phase slippage and Hohn et al[37] suggest that superconducting fluctuations due to reduced dimensionality may be an alternative mechanism.

1.2.4 Flux Structures and Dynamics in High T_c's

1.2.4.1 Vortex Structures and Quasi–2D Dimensionality

For YBCO with anisotropic coherence lengths of $\xi_c(0) \simeq 2$–3 Å, $\xi_{ab}(0) \simeq 15$ Å the inter planar spacing in the c direction lends to weak coupling in this direction. The 3D approximation of the standard Ginzburg–Landau model is only marginally justified except near T_c where ξ diverges as $(1-t)^{-1/2}$, with t the reduced temperature, $t \equiv T/T_c$. In Bismuth–based cuprates, (e.g. BSCCO), the 3D picture is not a good approximation at all since experiments have shown that anisotropy is at least an order of magnitude greater

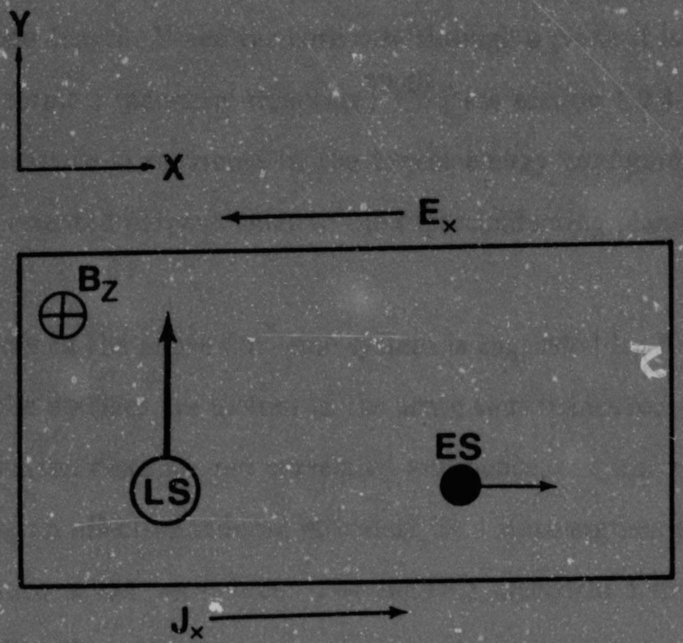

Figure 1.2.3. A superconducting circuit representing the relative motion of the extended states (ES) and the localised states (LS) resulting from an applied Lorentz force.

in BSCCO than in YBCO. A quasi–2D, Josephson coupled, system may be a better model for the equilibrium magnetic properties of the High–T_c's.[38] Due to the weak interplanar coupling it is energetically favourable for the magnetic vortices to lie in the interplanar spacing where the superconductivity is weaker. Complicated vortex structures are formed when the applied field is oriented at a slight angle to the ab plane vortices lie between the planes among most of their length. When the core cuts through a plane it is surrounded by circulating currents and forms a 'pancake' structure,[39,40] (see section 1.2.4.2 below). The characteristic Abrikosov lattice is recovered in the lowest energy configuration, occurring when the applied field is oriented perpendicular to the superconducting planes.

The possibilities of disorder in the above flux–line system is suggested by Freimuth et al,[41] in the assumption that the vortices are molten in the sense that 'pancakes' or vortex discs are well defined. These vortex discs are not correlated and hence, can move independently of one another, producing an effective induced electrical field since segments with opposite orientation do not produce a net zero force. The induced electrical field of these disc segments is in the same direction.

In single crystals, Abrikosov lattices have been observed at sufficiently low temperatures.[42] However, generally such patterns are not observed in good YBCO films; instead a random flux pattern is most often found. This pattern is characteristic of Fisher's[43] vortex–glass structure. The model predicts that in the presence of material disorder the vortex liquid at high temperatures will freeze into a disordered vortex glass state at low temperatures. Elemental vortex–vortex interactions should produce an ordered (archetypically hexagonal) lattice which becomes increasingly rigid for higher local inductions,

$$B_{local} = \left(\tfrac{2}{3}\right)^{1/2} \psi_o / a^2 \qquad 1.2.1$$

where a is the lattice spacing.

1.2.4.2 Flux Dynamics and Pinning in High–T_c Superconductors

At low temperatures, magnetic flux easily penetrates into the material along grain boundaries and intergranular vortices are formed which seemed to be pinned at the grain boundary discontinuities. Intragranular vortices are represented by a single vortex line composed of many Abrikosov 'pancakes' joined together by weak–link segments, pinned with different energies, (Figure 1.2.4). This picture of the vortex line is fundamental to the model proposed by Fischer[43]. Intragranular pinning results from the spatial inhomogeneities of the material, such as impurities, grain boundaries and dislocations. Pinning occurs at these sites since less energy is expended if a vortex core sits at a normal interface than if pair breaking must occur to achieve the same result. For High–T_c's the predominant pinning mechanism is an inter–granular, vortex–core pinning in which inhomogeneities should be of order ξ. Due to the very small values of the coherence lengths ($\simeq$ 10 A), vortex pinning sites possibly include oxygen vacancy–type positions and other atomic disorder that may arise from the complicated stoichiometry, twin boundaries, and other translational symmetry deviations. An extension to this **intrinsic pinning model** is suggested by Dolan et al.[42] For an applied field in the **ab** plane the vortex and associated fields, may cause the electronic structure of the adjacent planes, to alter, or alternatively cause a local disturbance in the superfluid, hence inducing its own potential minimum (pinning site).

The conventional model for **Flux creep**[10,44] has been extended to High–T_c's with suitable modification of the various superconducting parameters.[45] At low temperatures, where the contribution from $k_B T$ is small, and also in the presence of an excitation current that is considerably smaller than the pinning energies, the vortex motion displays Anderson's hopping from one pinning site to another. Flux creep occurs when the superconductor is in

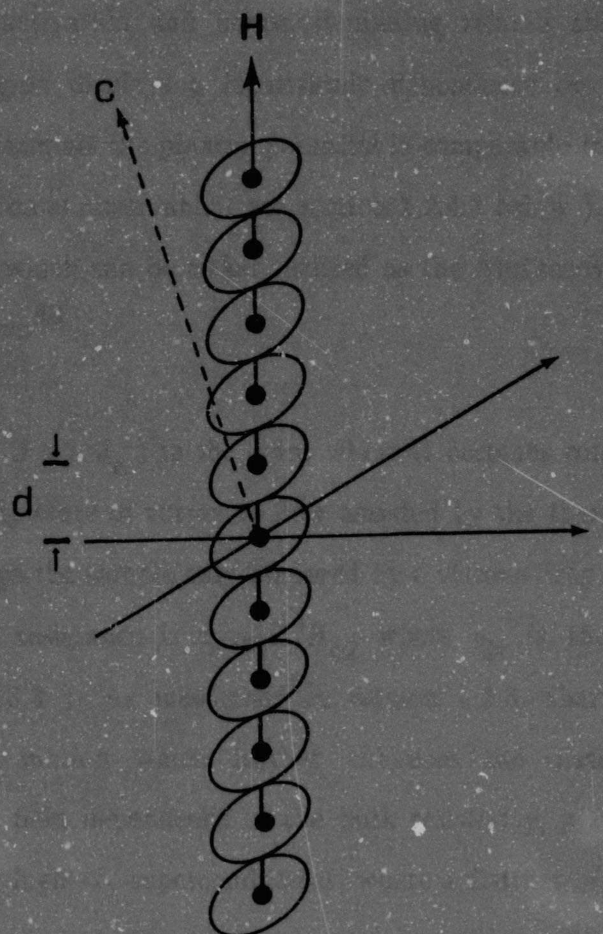

Figure 1.2.4 **Schematic of "pancake type" vortices that form in layered High–T_c materials due to the weak–interlayer coupling when a magnetic field penetrates the superconductor (below T_c in the mixed state) with a component normal to the ab planes. In the figure, H is the applied field, c indicates the c–axis and d is the interlayer spacing.**

a critical state ($J \simeq J_c$). At this critical state the magnetic flux readjusts itself until a maximum, and nearly constant gradient of B is reached. This critical state is not maintained as the thermal activation and hence, depinning relaxes this flux density gradient. The flux creep region displays a logarithmic dependence on J, in the I–V characteristics. In High–T_c materials the pinning potential is comparable to k_BT and even when $J << J_c$ the TAFF region is observable (see section 1.2.4.3 below). The flux creep occurs in a solid vortex state which can be either realised as the Abrikosov lattice or as a glass state considered by Fischer.[43]

Increasing the Lorentz force ($J >> J_c$) to the point where it becomes comparable to the pinning energy, causes a steady state of vortex to flow assisted by the thermal activation. The vortex liquid flows through the sample only hindered by a viscous drag. This motion is the **flux flow** state and the resistance is $\simeq \rho_N H/H_{c2}$ where ρ_N is the normal state resistivity, (see section 1.1.3.3). As mentioned in section 1.2.3, thermal heating is associated with this vortex motion which further enhances the dissipation of the superconducting sample. The field dependence of the bulk resistivity, $\rho(H)$, for the flux flow region is most notable for high–T_c superconductors, where a distinct broadening of the transition and earlier onset of dissipation is evident. (see Figure 1.2.5). $\rho(H)$ for conventional systems is included as a comparison. In these systems very slight, if any, rounding of the transition occurs; the position of T_c merely moves to the left of the temperature scale, with increasing field.

1.2.4.3 Thermally Activated Flux Flow (TAFF)

In the Anderson and Kim[46] model they describe the hopping of flux bundles in the direction of the Lorentz force, due to thermal activations. In high–T_c's due to the very high critical temperatures, the available thermal energy, k_BT, is an order of magnitude

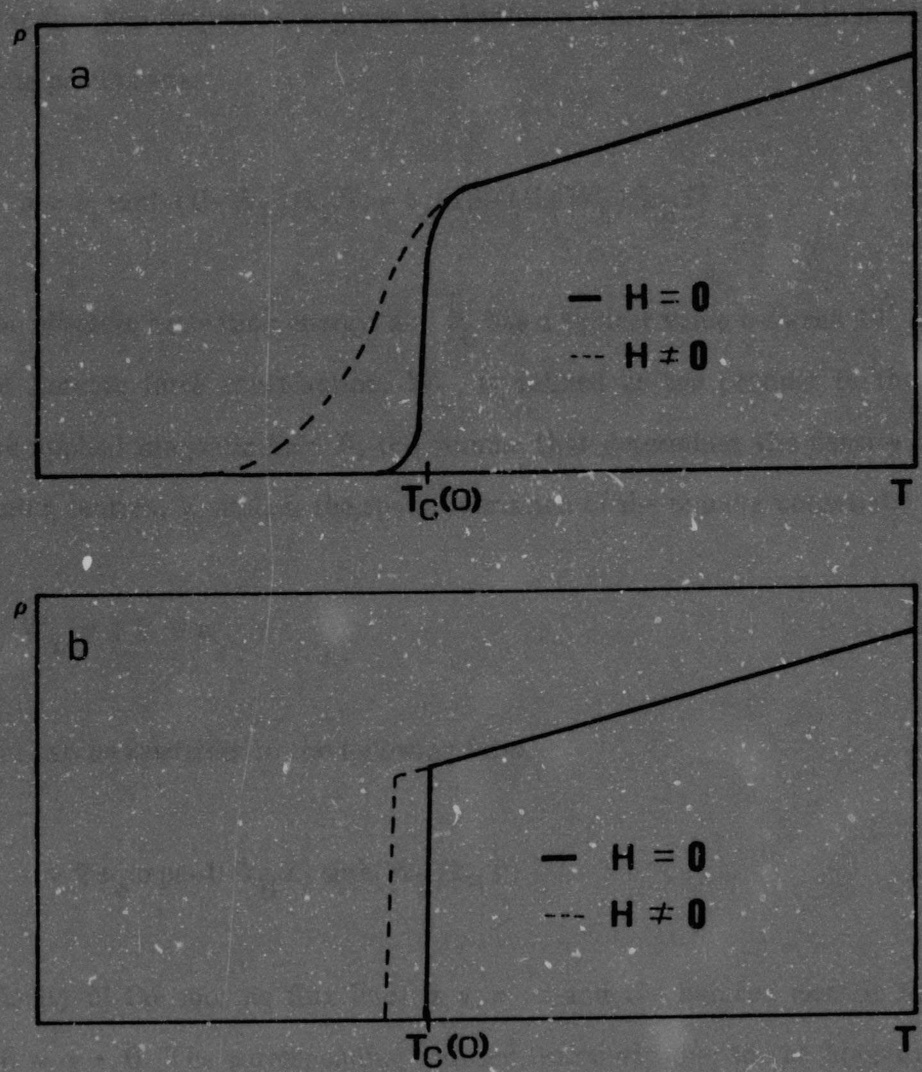

Figure 1.2.5 A comparison of the magnetic field dependent resistivity, $\rho(H)$, for a) High–T_c superconductors and b) conventional systems. The characteristic rounding and broadening of the transition in High–Tc's, is compared to the temperature shift in the region of transition for conventional systems.

sample allows for flux bundles to move (hop), in an opposite direction to the Lorentz force.[46,47] The flux hop frequency, ν, given by Anderson must be extended to include these reverse hopping phenomena:

$$\nu = \nu_0 \exp[-(U-W_L)/k_BT] - \nu_0 \exp[-(U+W_L)/k_BT] \qquad 1.2.2$$

where U is the effective activation energy, and ν_0 has a typical value between 10^7 and 10^{11} Hertz.[48] The Lorentz force contribution, W_L, is defined as the product of the current density J, the applied magnetic field B, the volume that determines the density of states acting as pinning centres, V, and, a, the spatial variation of the pinning potential:

$$W_L = J\,B\,V\,a \qquad 1.2.3$$

Equation 1.2.2 can be rewritten in the following form,

$$\nu = 2\,\nu_0 \exp(-U/k_BT)\sinh(W_L/k_BT) \qquad 1.2.4$$

The drift velocity of the moving flux lines is $\mathbf{v} = \nu a$ and the induced electric field from Faraday is, $\mathbf{E} = \mathbf{v} \times \mathbf{B}$. The corresponding induced resistivity due to the hopping of flux lines is,

$$\rho = (2\nu_0 Ba/J)\exp(-U/k_BT)\sinh(W/k_BT) \qquad 1.2.5$$

For small currents, the Lorentz force, $W_L << k_BT$ and the hyperbolic term can be approximated as $\sinh(W_L/k_BT) \simeq W_L/k_BT$. Substituting for W_L, the hopping resistivity reduces to,